SUPPORTING INFORMATION FOR

Platinum(II) Alkyl Complexes of Chelating Dibridgehead Diphosphines $P((CH_2)_n)_3P$ (n = 14, 18, 22); Facile *cis*/*trans* Isomerizations Interconverting Gyroscope and Parachute like Adducts

Yun Zhu,[℘] Andreas Ehnbom,[℘] Tobias Fiedler,[‡℘] Yi Shu, Nattamai Bhuvanesh,
Michael B. Hall,[*℘] and John A. Gladysz[*℘]

Department of Chemistry, Texas A&M University, PO Box 30012, College Station, Texas
77842-3012, USA

for publication in *Dalton Transactions*

■ Additional crystallographic data

The three independent molecules found in the unit cell of crystalline *trans*-**7c** are depicted in Figure s01.

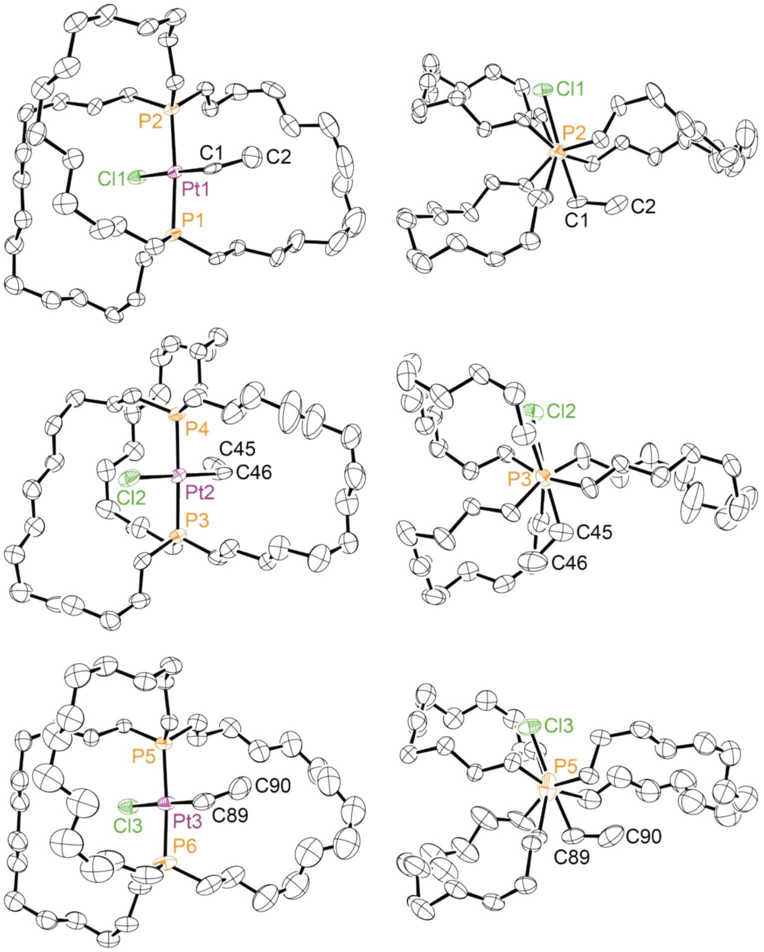

Figure s01. Thermal ellipsoid plots of the molecular structure of *trans*-**7c** (50% probability level, three independent molecules).

■ Computational Section

1. General considerations. The general computational methodology employed is outlined in Figure s02. The conformational spaces of all species were first sampled using molecular mechanics and simulated annealing (MM/MD), following a protocol reported in an earlier study.[s01] This method is fast and has the ability to sample hundreds of thousands of conformations; however, the inherent level of theory is based on force fields. Several of the structures were submitted for Born Oppenheimer Molecular Dynamics (BOMD) (QM/MD), where the forces for the Newtonian trajectories are computed in each time frame (on-the-fly) using Density Functional Theory (DFT).[s02,s03] Because the end results varied very little between the techniques, the BOMD data will not be presented.

Structures were sampled and extracted from both techniques and were further optimized using DFT (see section 5 for a benchmark study and section 6 for additional DFT details). The same level of theory in the DFT optimizations was used in the BOMD calculations. Ten low-energy conformations throughout each trajectory were extracted from the MM/MD simulated annealing simulation for subsequent DFT optimization. The MD simulations allow sampling of structures over time, and at elevated temperatures, matching experimental conditions.

All extracted structures were subjected to DFT optimizations (in the gas phase) at the B3LYP/6-311+G(d) level of theory.[s04,s05] Grimme's dispersion corrections (GD3BJ) were crucial to establish conformations also found crystallographically.[s01b,s06] An ultrafine grid, (routeline command "int=ultrafine"), which is the default in Gaussian 16, was employed.[s07] Subsequent single point corrections using implicit solvent models (SMD) in toluene and *o*-$C_6H_4Cl_2$ (in addition to gas phase) were performed.[s08] All DFT extracted species were also separately subjected to frequency calculations and the statistical mechanical corrections were made for $T = 298$ and 414 K [141 °C]. The results are plotted in the main text (Figures 5 and 6) for the full complexes and acyclic models, respectively.

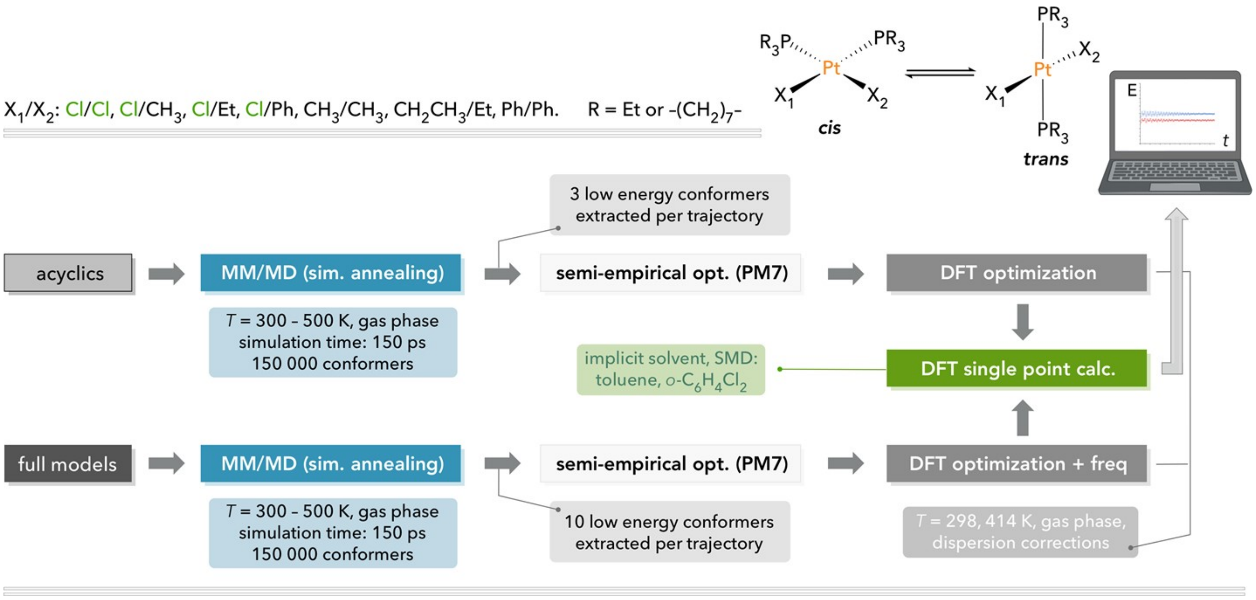

Figure s02. A graphical overview of the computational sequence used in this study.

Due to the elevated temperature, and thus access to higher vibrational modes, certain bonds can be elongated in the extracted structures (in particular for the modern BOMD method). Thus, a semiempirical (PM7) optimization was performed on all extracted species from the QM/MD and MM/MD simulations computations before subjecting them to DFT optimizations, in order to accelerate the latter.[s09]

2. Details of the simulated annealing (MM/MD) calculations: The simulated annealing calculations employed the Forcite module in MaterialsStudio™ with NVT ensembles using random initial velocities, initial temperatures of 300 K, mid-cycle temperatures of 500 K, 5 heating ramps per cycle, and 10,000 dynamic steps per ramp.[s10] Thus, the total number of steps was 15,000,000. The sampled structures were automatically geometry optimized after each cycle using the smart algorithm with a "fine" convergence tolerance (energy of 0.0001 kcal/mol, force of 0.005 kcal/mol·Å, displacement of 0.00005 Å, maximum of 10,000 iterations). The time steps in the annealing cycles were 1.0 femtoseconds, generating a total simulation time of 150 nanoseconds. The universal force fields[s11] (UFF) was used with atom based electrostatics *and* van der Waals terms using cubic spline truncation, cutoff distances of 15.5 Å, spline widths of 1.0 Å, and buffer widths of 0.5 Å.

3. Simulated annealing MM/MD data: The generated annealing MM/MD data for *cis* (×) and *trans* (○) platinum species *cis*/*trans*-**5c**, **7c**, **8c**, **4c**, **6c**, **3c** are given in the same plot (Figures s03 and s04). Each panel represents a different complex, and all were run in the gas phase. These data show that there is a large conformational space for each isomer at the 17-membered macrocycle size (n = 14). It was found that this MD technique distorts and samples the conformational space better than the BOMD technique. This is presumably caused by the larger temperature range of the simulated annealing setup, subjecting species to cycling temperatures ranging from 300 to 500 K. The drawback of this methodology is that only gas phase calculations are available in the computational suite in MaterialsStudio. Thus, it was decided to further pursue calculations using BOMD, although, only for evaluative purposes (i.e. quality assurance). The MM/MD data in Figures s03-s06 shows the potential energy plotted in units of kcal/mol versus the simulation time in femtoseconds.

GaussView 6.1.1[s12] was used to study the different trajectories and VMD 1.9.3[s13] was used to generate videos. CylView 1.0[s14] was used to visualize specific frames and computational models throughout the study, including the DFT data.

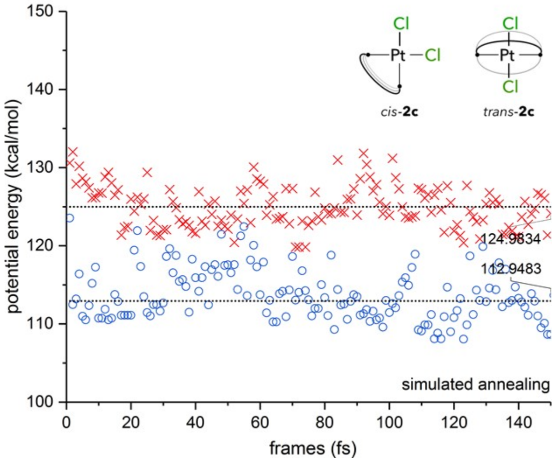

Figure s03. Molecular dynamics simulations (MM/MD, simulated annealing) of *cis*-**2c** (×) and *trans*-**2c** (○). The trajectories are run in the gas phase.

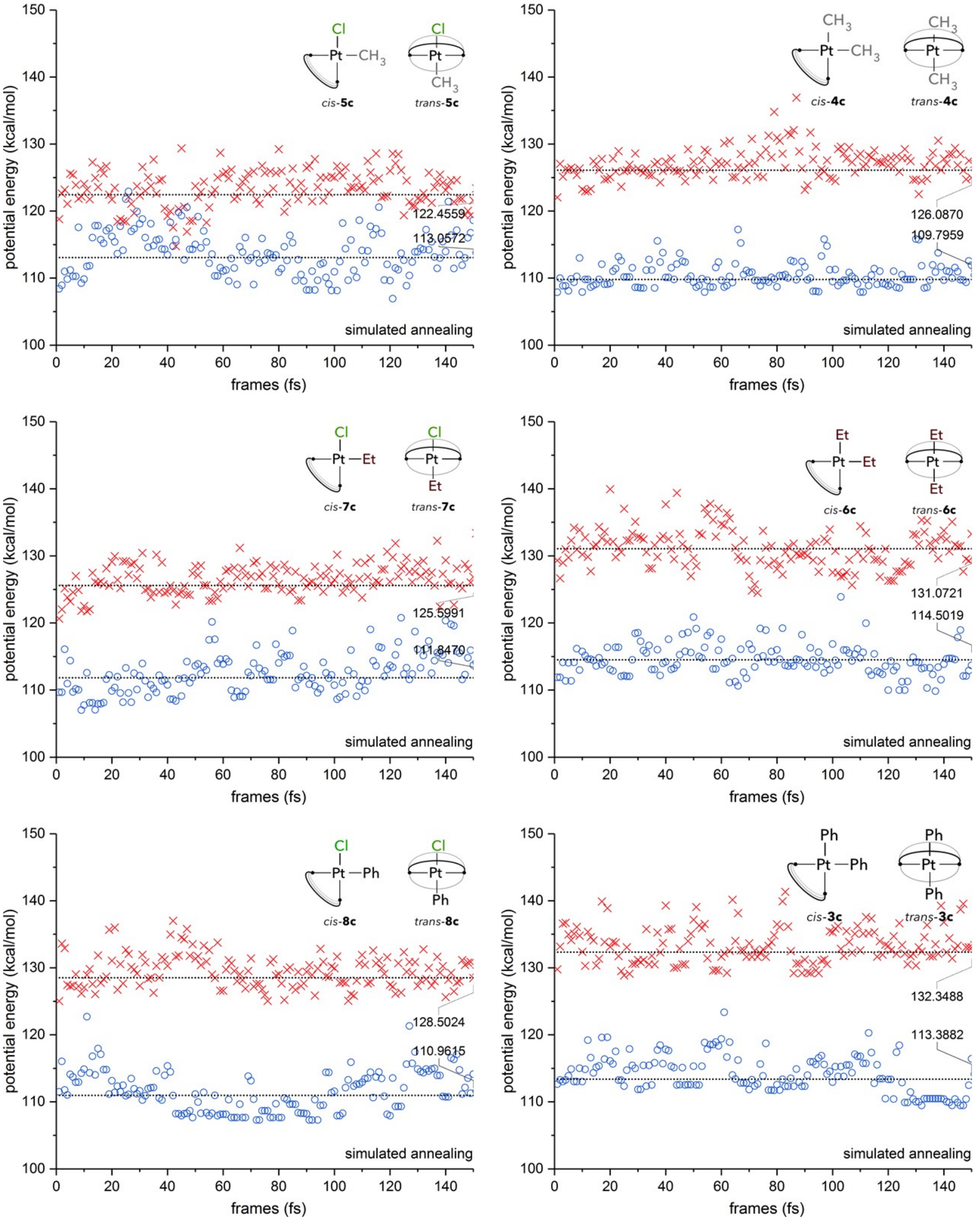

Figure s04. Molecular dynamics simulations (MM/MD, simulated annealing) of *cis*/*trans*-**5c**, **7c**, **8**, **4c**, **6c**, **3c**. The trajectories are run in the gas phase.

Truncated models using $P(CH_2CH_3)_3$ ligands were constructed to understand electronic effects and avoid bias from macrocyclic cages with large degrees of freedom. The simpler $P(CH_3)_3$ analogue could have been used; however, the electronic effect exerted by $P(CH_2)_{14}$ is better represented by $P(CH_2CH_3)_3$.[s15] These species were subjected to the same type of calculation conditions as the full models discussed in the preceding sections (see Figures s05 and s06 for the results). This allows one to accurately map the electronic contributions of different ligands.

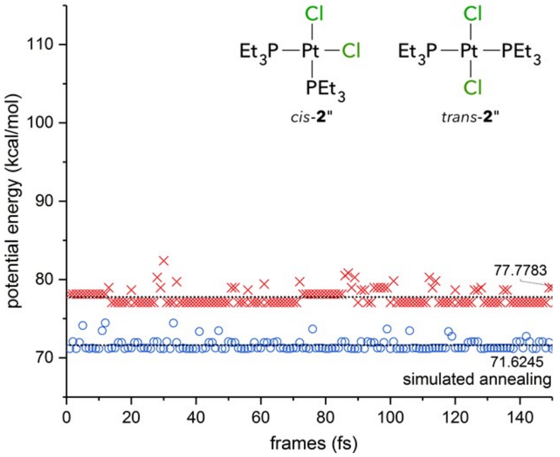

Figure s05. Molecular dynamics simulations (MM/MD, simulated annealing) of acyclic *cis*-**2"** (×) and *trans*-**2"** (○). The trajectories are run in the gas phase.

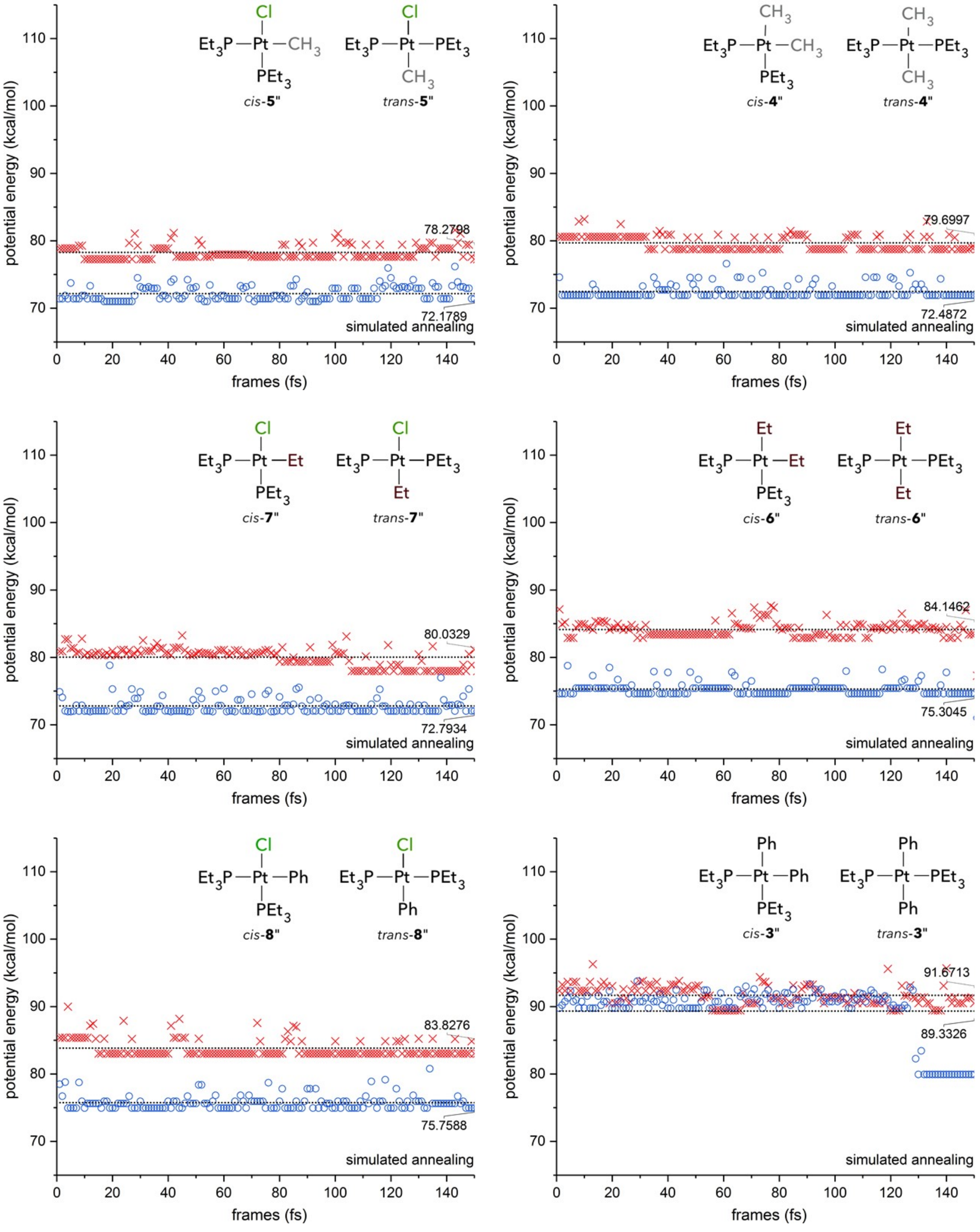

Figure s06. Molecular dynamics simulations (MM/MD, simulated annealing) of acyclic *cis*/*trans*-**5**", **7**", **8**", **4**", **6**", **3**". The trajectories are run in the gas phase.

4. Details of the Born-Oppenheimer molecular dynamics (DFT/MD) simulations: The Born-Oppenheimer molecular dynamics (BOMD) simulations were performed at the B3LYP-GD3BJ/6-311+G(d)[s04,s05] level of theory, and were only run for evaluative purposes (i.e. quality assurance of the MM/MD data). A fully relativistic effective core potential (ECP60MDF) paired with a correlation consistent triple ζ quality basis set (cc-pVTZ-PP) was used on the platinum atom.[s16] A benchmark study for the selected DFT level of theory is provided in section 5 and additional DFT details are found in section 6. Useful protocols for BOMD calculations featuring direct examples can be found in the supplementary information of references [s02] and [s03]. Relevant information has been provided below. The BOMD calculations were all performed at temperatures (T = 141 °C) and solvents (toluene, o-$C_6H_4Cl_2$), in addition to the gas phase.

In the currently used implementation of BOMD in Gaussian, all forces are quantum mechanically evaluated at each frame (using DFT). The BOMD calculations use the same level of theory as in the separate DFT optimizations (see section 6). The nuclear motion is non-quantized and the velocity Verlet integration algorithm is applied to the Newtonian equations of motion. A microcanonical ensemble is responsible for the propagation of the trajectories. Thus, the total energy (the sum of potential E_p and kinetic energy E_k) is conserved, as is the number of particles N and volume V. A random Maxwell-Boltzmann distribution assigns the initial velocity of each atom with E_k being adjusted depending on the simulation temperature (T = 414 K, 140 °C which was set to match the experimental conditions). The zero point energy is not included in these calculations.

The temperature was implemented through the keyword "nke" (initial kinetic energy) as there is currently no implemented temperature thermostat in Gaussian. Equation (1) was used where N_Atoms is the total number of atoms of the system, k is the Boltzmann constant, and T is the given temperature.

$$\$nke = \left(N_\mathrm{Atoms} - 1\right) \times \frac{3}{2} kT \qquad \text{(eq. 1)}$$

The following generic routeline exemplifies the different parameters used in the BOMD calculations.

```
#p B3LYP/genecp iop(1/44=$random_seed) BOMD(gradientonly, stepsize=$n, sample=microcanonical, randomvelocity, maxpoints=$maxpoint, nke=$nke) empiricaldispersion=GD3BJ scrf=(smd,solvent=S), int=ultrafine.
```

$*random_seed* determines the random number generation seeds. $maxpoint is the total simulation time and one femtosecond step size is used. *S* is the given solvent, which in this study is toluene or *o*-$C_6H_4Cl_2$.

5. Benchmark study: A benchmark study was performed on the smallest *cis* and *trans* species carrying no chelating ligand, i.e. Cl/Cl, Cl/CH$_3$, and CH$_3$/CH$_3$, all with P(CH$_3$)$_3$. The data are recorded in Table s01. A variety of functionals and different families of basis sets were used. The data conclusively demonstrate that the choice of functional does not impact the energetic drastically and that the accuracy of the previously used level of theory [B3LYP-GD3BJ/6-311+G(d)] is sufficient to determine the relative energetics.

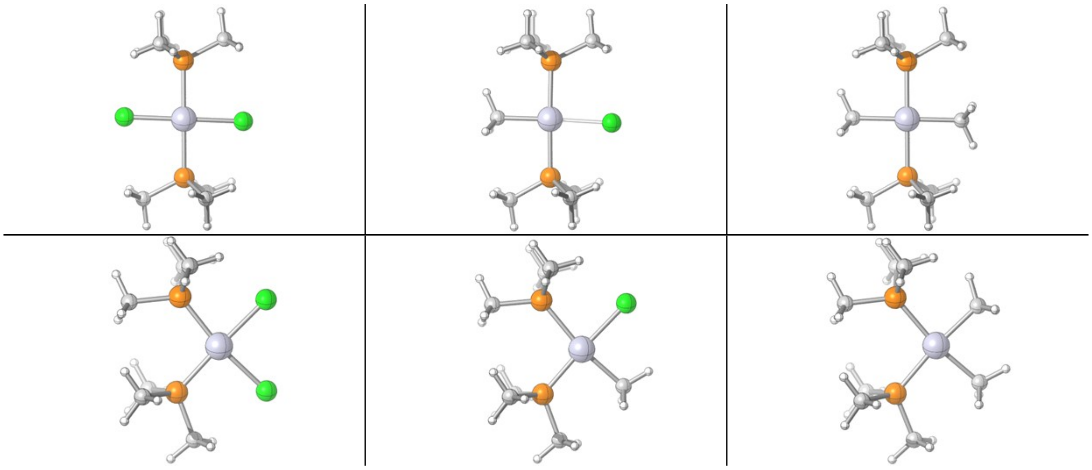

Table s01. Key pairs of *cis*/*trans* species with computed stability differences (kcal/mol).

functional	basis set[a]	solvent[b]	dispersion correction[c]	Cl/Cl[d] (*cis* vs. *trans*)	Cl/CH$_3$[d] (*cis* vs. *trans*)	CH$_3$/CH$_3$[d] (*cis* vs. *trans*)
B3LYP	6-311+G(*d*)	gas	GD3BJ	–6.0	–5.3	2.3
TPSS	6-311+G(*d*)	gas	GD3BJ	–4.2	–3.9	3.4
CAM-B3LYP	6-311+G(*d*)	gas	GD3BJ	–7.0	–5.9	1.6
M06	6-311+G(*d*)	gas	GD3	–6.7	–5.3	2.3
B3LYP	6-311+G(*d*)	H$_2$O	GD3BJ	6.1	–1.4	3.4
B3LYP	6-311+G(*d*)	C$_6$H$_6$	GD3BJ	–1.6	–4.3	2.4
B3LYP	6-311+G(*d*)	Et$_2$O	GD3BJ	1.2	–3.3	2.7
B3LYP	6-311++G(*d*)	gas	GD3BJ	–6.0	–5.3	2.4
B3LYP	6-311++G(2*d*,2*p*)	gas	GD3BJ	–5.2	–5.0	2.1
B3LYP	def2-SVP	gas	GD3BJ	–5.1	–4.8	2.4
B3LYP	def2-TZVP	gas	GD3BJ	–4.4	–4.5	2.0
B3LYP	def2-QZVP	gas	GD3BJ	–4.3	–4.6	1.8
B3LYP	cc-PVDZ	gas	GD3BJ	–5.6	–5.2	2.6
B3LYP	cc-PVQZ	gas	GD3BJ	–4.5	–4.6	2.0
ωB97X-D	6-311+G(*d*)	gas	—	–6.8	–5.9	1.6

[a] The platinum atom was fitted with a triple-ζ quality basis set (cc-pVTZ-PP) paired with a fully relativistic effective core potential (ECP60MDF). [a] Truhlar's universal continuum solvation model (SMD) was used.[s08] [c] Grimme's empirical dispersion corrections with Becke-Johnson damping were used in all applicable cases except for incompatible functionals. [d] Relative total electronic energy between the *cis*/*trans* species in which the *cis* dichloride, monochloride, and dimethyl complexes are set to zero (0 kcal/mol).

6. Electronic structure theory, DFT: Electronic structure calculations employed the Gaussian16™ (revision C.01) program package using the ultrafine grid (99,590) to enhance accuracy.[s07] Gas phase geometries were optimized using DFT. The B3LYP[s04] functional was paired with an all-electron triple ζ quality 6-311+G(d)[s05] basis set on all atoms except platinum. For platinum a fully relativistic effective core potential (ECP60MDF) was paired with a correlation consistent triple ζ quality basis set (cc-pVTZ-PP).[s16] The choice of functional and basis set was based on a previous study for similar structures where good agreement was reached between experiment and theory (structural and energetic data). A benchmark study (section 5) was further undertaken to showcase that there were small variations in relative energies among commonly used functionals and even higher quality basis set. Dispersion corrections were implemented using the D3 version of Grimme's dispersion function with Becke-Johnson damping (referred to as GD3BJ).[s06] These are critical for the correct folding of the ligand scaffolds as can be shown in the model structure below (Figure s07). A sample input file for an optimization is provided after the reference section.

Selected computed structures (one conformation per complex) are provided in a separate concatenated xyz formatted text file (optimized_structures.xyz), which can be easily opened using a variety of free software, e.g. Mercury.[s17] The bond distance data provided in Figure 7 is based on an average of three computed conformers per complex.

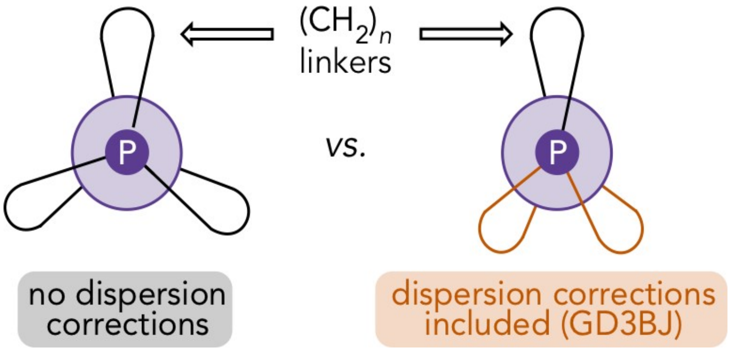

Figure s07. Views of gyroscope like complexes showing attractions between two $(CH_2)_n$ bridges if dispersion corrections are used.

7. Energetics of excised diphosphine ligands, single point calculation (DFT): To further probe the origin of the energy differences associated with the *cis*/parachute and *trans*/gyroscope isomers (ca. 6.6 kcal/mol with $(CH_2)_{14}$ bridges; see Figures 5 and 6), and respond to a reviewer inquiry, additional computations involving $P((CH_2)_{14})_3P$, $H_2P(CH_2)_{14}PH_2$ and $HP((CH_2)_{14})_2PH$ species were submitted. First, the PtX_2 or PtXX' fragments were excised from the complexes in Figure 5, leaving only the $P((CH_2)_{14})_3P$ scaffolds. These were computed at the same level of theory as in the preceding DFT investigations, but only single-point calculations were performed, keeping all atoms fixed. The relative electronic energies of the $P((CH_2)_{14})_3P$ species stemming from the *cis*/*trans* complexes are presented in Figure s08 (average difference = –4.6 kcal/mol). Note that only *one* of the 10 conformers from each complex was computed. The PtX_2 or PtXX' fragment designations are retained in Figure s08 to identify the complex of origin.

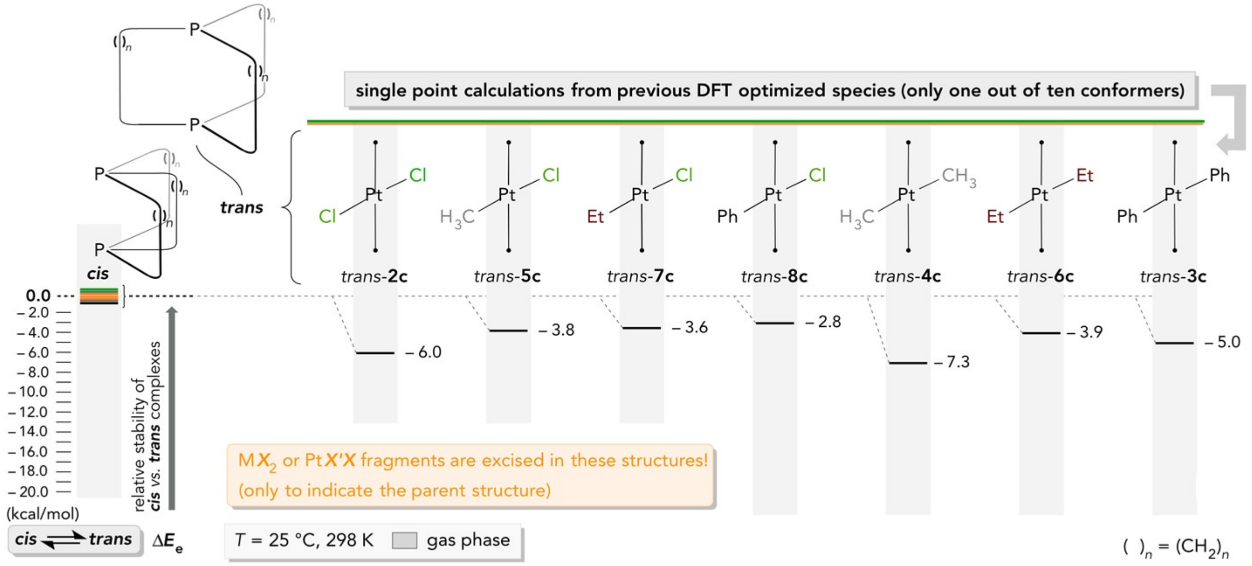

Figure s08. Structures and relative electronic energies from single point energy calculations on $P((CH_2)_{14})_3P$ scaffolds excised from the platinum complexes indicated.

Next, single-point calculations on the $H_2P(CH_2)_{14}PH_2$ and $HP((CH_2)_{14})_2PH$ systems derived from *cis*/*trans*-**2c** were carried out. The electronic energy differences between the *cis*/*trans* species are shown in Figure s09, together with the "three stranded" $P((CH_2)_{14})_3P$ species from *cis*/*trans*-**2c**. The energetic differences are minimal in $H_2P(CH_2)_{14}PH_2$, but much greater in both the $HP((CH_2)_{14})_2PH$ and $P((CH_2)_{14})_3P$ systems. In all equations, *trans* isomers are favored. This suggests that interactions between the chains are important for understanding energetic differences in these diphosphine scaffolds.

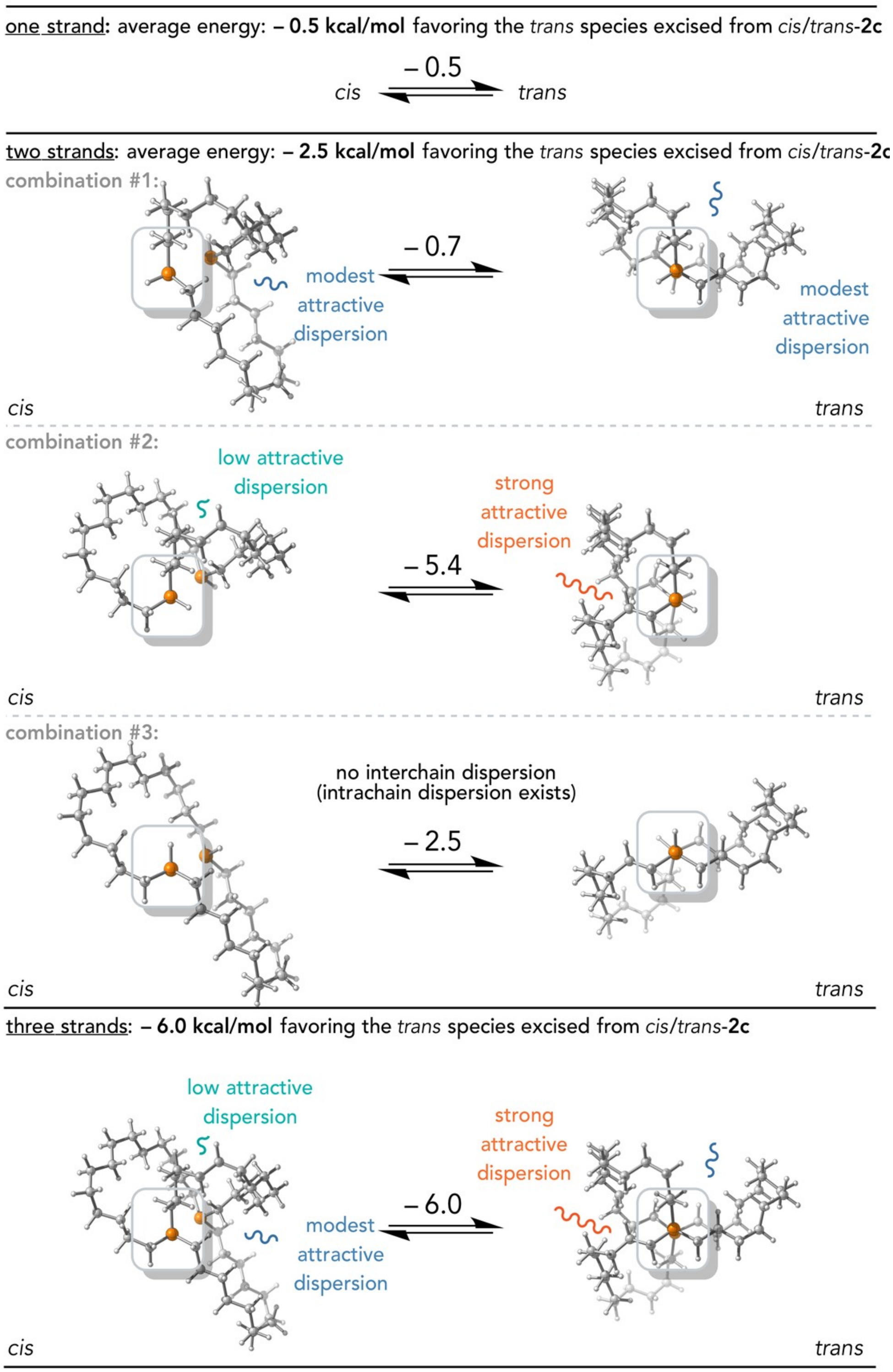

Figure s09. Structures and relative electronic energies from single point energy calculations of the diphosphines $H_2P(CH_2)_{14}PH_2$, $HP((CH_2)_{14})_2PH$, and $P((CH_2)_{14})_3P$ derived from the parent platinum complexes *cis*/*trans*-**2c**.

■ REFERENCES

(s01) Joshi, H.; Kharel, S.; Ehnbom, A.; Skopek, K.; Hess, G. D.; Fiedler, T.; Hampel, F.; Bhuvanesh, N.; Gladysz, J. A. Three-Fold Intramolecular Ring Closing Alkene Metatheses of Square Planar Complexes with *cis* Phosphorus Donor Ligands $P(X(CH_2)_mCH{=}CH_2)_3$ (X = —, *m* = 5–10; X = O, *m* = 3–5): Syntheses, Structures, and Thermal Properties of Macrocyclic Dibridgehead Diphosphorus Complexes. *J. Am. Chem. Soc.* **2018**, *140*, 8463-8478.

(s02) Pu, M.; Sanhueza, I. A.; Senol, E.; Schoenebeck, F. Divergent Reactivity of Stannane and Silane in the Trifluoromethylation of Pd^{II}: Cyclic Transition State versus Difluorocarbene Release. *Angew. Chem. Int. Ed.* **2018**, *57*, 15081-15085.

(s03) Scattolin, T.; Pu, M.; Schoenebeck, F. Investigation of $(Me_4N)SCF_3$ as a Stable, Solid and Safe Reservoir for $S{=}CF_2$ as a Surrogate for Thiophosgene. *Chem. Eur. J.* **2018**, *24*, 567-571.

(s04) (a) Becke, A. D. Density-functional exchange-energy approximation with correct asymptotic behavior. *Phys. Rev. A*, **1988**, *38*, 3098-3100. (b) Becke, A. D. Density-functional thermochemistry. III. The role of exact exchange. *J. Chem. Phys.* **1993**, *98*, 5648-5652. (c) Lee, C.; Yang, W.; Parr, R. G. Development of the Colle-Salvetti correlation energy formula into a functional of the electron density. *Phys. Rev. B*, **1988**, *37*, 785-789.

(s05) Pople basis set reference for "6-311G". An addition of "d" adds polarization functions of *d*-type to C, "p" adds *p*-type polarization functions to C and H atoms. "+/++" indicates added diffuse functions: (a) McLean, A. D.; Chandler, G. S. Contracted Gaussian basis sets for molecular calculations. I. Second row atoms, Z = 11-18. *J. Chem. Phys.* **1980**, *72*, 5639-5648. (b) Raghavachari, K.; Binkley, J. S.; Seeger, R.; Pople, J. A. Self-consistent molecular orbital methods. XX. A basis set for correlated wave functions. *J. Chem. Phys.* **1980**, *72*, 650-654.

(s06) Grimme, S.; Ehrlich, S.; Goerigk, L. Effect of the damping function in dispersion corrected density functional theory. *J. Comput. Chem.* **2011**, *32*, 1456-1465.

(s07) Gaussian 16, *Revision C.01*, Frisch, M. J.; Trucks, G. W.; Schlegel, H. B.; Scuseria, G. E.; Robb, M. A.; Cheeseman, J. R.; Scalmani, G.; Barone, V.; Petersson, G. A.; Nakatsuji, H.; Li, X.; Caricato, M.; Marenich, A. V.; Bloino, J.; Janesko, B. G.; Gomperts, R.; Mennucci, B.; Hratchian, H. P.; Ortiz, J. V.; Izmaylov, A. F.; Sonnenberg, J. L.; Williams-Young, D.; Ding, F.; Lipparini, F.; Egidi, F.; Goings, J.; Peng, B.; Petrone, A.; Henderson, T.; Ranasinghe, D.; Zakrzewski, V. G.; Gao, J.; Rega, N.; Zheng, G.; Liang, W.; Hada, M.; Ehara, M.; Toyota, K.; Fukuda, R.; Hasegawa, J.; Ishida, M.; Nakajima, T.; Honda, Y.; Kitao, O.; Nakai, H.; Vreven, T.; Throssell, K.; Montgomery, J. A., Jr.; Peralta, J. E.; Ogliaro, F.; Bearpark, M. J.; Heyd, J. J.; Brothers, E. N.; Kudin, K. N.; Staroverov, V. N.; Keith, T. A.; Kobayashi, R.; Normand, J.; Raghavachari, K.; Rendell, A. P.; Burant, J. C.; Iyengar, S. S.; Tomasi, J.; Cossi, M.; Millam, J. M.; Klene, M.; Adamo, C.; Cammi, R.; Ochterski, J. W.; Martin, R. L.; Morokuma, K.; Farkas, O.; Foresman, J. B.; Fox, D. J. Gaussian, Inc., Wallingford CT, **2016**.

(s08) Marenich, A. V.; Cramer, C. J.; Truhlar, D. G. Universal Solvation Model Based on Solute Electron Density and on a Continuum Model of the Solvent Defined by the Bulk Dielectric Constant and Atomic Surface Tensions. *J. Phys. Chem. B*. **2009**, *113*, 6378-6396.

(s09) PM7 (a) Christensen, A. S.; Kubař, T.; Cui, Q.; Elstner, M. Semiempirical Quantum Mechanical Methods for Noncovalent Interactions for Chemical and Biochemical Applications. *Chem. Rev.* **2016**, *116*, 5301-5337. (b) Stewart, J. J. P. Optimization of parameters for semiempirical methods VI: more modifications to the NDDO approximations and re-optimization of parameters. *J. Mol. Model.* **2013**, *19*, 1-32.

(s10) Dassault Systèmes BIOVIA, Materials Studio, 6.0, San Diego: Dassault Systèmes, 2017.

(s11) Rappé, A. K.; Casewit, C. J.; Colwell, K. S.; W. A. Goddard III, W. A.; Skiff, W. M. UFF, a full periodic-table force field for molecular mechanics and molecular-dynamics simulations. *J. Am. Chem. Soc.* **1992**, *114*, 10024-10035.

(s12) GaussView, Version 6.1.1, Roy Dennington, Todd Keith, and John Millam, Semichem Inc., Shawnee Mission, KS, 2019.

(s13) Humphrey, W., Dalke, A. and Schulten, K., "VMD - Visual Molecular Dynamics", *J. Molec. Graphics*, **1996**, vol. 14, pp. 33-38. (http://www.ks.uiuc.edu/Research/vmd/)

(s14) CYLview, 1.0b; Legault, C. Y., Université de Sherbrooke, 2009 (http://www.cylview.org)

(s15) (a) Suresh, C. H.; Koga, N.; Quantifying the Electronic Effect of Substituted Phosphine Ligands via Molecular Electrostatic Potential. *Inorg. Chem.* **2002**, *41*, 1573-1578. (b) Tolman, C. A. Steric effects of phosphorus ligands in organometallic chemistry and homogeneous catalysis. *Chem. Rev.* **1977**, *77*, 313-348.

(s16) Figgen, D.; Peterson, K. A.; Dolg, M. Energy-consistent pseudopotentials and correlation consistent basis sets for the 5*d* elements Hf–Pt. *J. Phys. Chem.* **2009**, *130*, 164108.

(s17) Macrae, C. F.; Bruno, I. J.; Chisholm, J. A.; Edgington, P. R.; McCabe, P.; Pidcock, E.; Rodriguez-Monge, L.; Taylor, R.; van de Streek, J.; Wood, P. A. Mercury CSD 2.0 – new features for the visualization and investigation of crystal structures. *J. Appl. Crystallogr.* **2008**, *41*, 466-470.

Appendix A

SAMPLE INPUT DFT OPTIMIZATION/FREQUENCY FILE

```
%chk=/path/filename.chk
#p opt freq b3lyp/genecp empiricaldispersion=gd3bj int=(ultrafine,acc2e=11) iop(1/8=10)

Title

0 1
 Pt             0.27790000   -1.35650000   -0.04900000
 P             -0.29220784   -0.17782508    1.98946632
… [truncation of XYZ coordinates]
H              -0.58949506   -0.95725571   -3.46489122
 Cl             0.79059916   -2.83074388   -1.71097008
 Cl             0.22834629   -3.24969108    1.22055581

Pt 0
YYY
****
C P H Cl 0
6-311g(d)
****

Pt 0
ZZZ
```

Replace *YYY* with:

```
Pt 0
S 10 1.00
0.36006400E+02 0.15603000E-01
0.22499100E+02 -0.13960000E+00
0.14060900E+02 0.39946900E+00
0.87816100E+01 -0.12774400E+00
0.49923800E+01 -0.75145100E+00
0.13838500E+01 0.86332700E+00
0.66161700E+00 0.49759400E+00
0.20488200E+00 0.34758000E-01
0.92230000E-01 -0.65890000E-02
0.39264000E-01 0.27160000E-02
S 10 1.00
0.36006400E+02 -0.56780000E-02
0.22499100E+02 0.50755000E-01
0.14060900E+02 -0.15003000E+00
0.87816100E+01 0.63982000E-01
0.49923800E+01 0.27041100E+00
0.13838500E+01 -0.43465700E+00
0.66161700E+00 -0.33729000E+00
0.20488200E+00 0.28144600E+00
0.92230000E-01 0.64557900E+00
0.39264000E-01 0.29695500E+00
S 10 1.00
0.36006400E+02 0.70370000E-02
0.22499100E+02 0.10525000E-01
0.14060900E+02 -0.85498000E-01
0.87816100E+01 -0.17655900E+00
0.49923800E+01 0.85670700E+00
0.13838500E+01 -0.18442100E+01
0.66161700E+00 0.60115600E+00
0.20488200E+00 0.19822930E+01
0.92230000E-01 -0.11764800E+01
0.39264000E-01 -0.46329100E+00
S 10 1.00
0.36006400E+02 -0.11445000E-01
0.22499100E+02 0.12204400E+00
0.14060900E+02 -0.37590600E+00
0.87816100E+01 0.55388000E-01
0.49923800E+01 0.11335870E+01
0.13838500E+01 -0.42149190E+01
0.66161700E+00 0.48759410E+01
0.20488200E+00 -0.21659360E+01
0.92230000E-01 -0.42680400E+00
0.39264000E-01 0.11220650E+01
S 1 1.00
0.39264000E-01 1.0
P 9 1.00
0.21598600E+02 -0.12515000E-01
0.13516000E+02 0.71570000E-01
0.59203700E+01 -0.28727600E+00
0.16412600E+01 0.51541900E+00
0.83113100E+00 0.48046100E+00
0.40843000E+00 0.16799600E+00
0.17542700E+00 0.15860000E-01
0.72685000E-01 0.79500000E-03
0.29761000E-01 -0.10000000E-05
P 9 1.00
0.21598600E+02 0.29600000E-02
0.13516000E+02 -0.19110000E-01
0.59203700E+01 0.83898000E-01
0.16412600E+01 -0.18300900E+00
0.83113100E+00 -0.18788400E+00
0.40843000E+00 -0.17870000E-02
0.17542700E+00 0.36067100E+00
0.72685000E-01 0.54492100E+00
0.29761000E-01 0.23693600E+00
P 9 1.00
0.21598600E+02 0.67690000E-02
0.13516000E+02 -0.42940000E-01
0.59203700E+01 0.18945500E+00
0.16412600E+01 -0.46064700E+00
0.83113100E+00 -0.44633500E+00
0.40843000E+00 0.48968400E+00
0.17542700E+00 0.68258800E+00
0.72685000E-01 0.12794700E+00
0.29761000E-01 0.25720000E-02
```

```
P 9 1.00
0.21598600E+02 0.11651000E-01
0.13516000E+02 -0.71522000E-01
0.59203700E+01 0.32596400E+00
0.16412600E+01 -0.12148310E+01
0.83113100E+00 0.15872700E+00
0.40843000E+00 0.15953330E+01
0.17542700E+00 -0.77793300E+00
0.72685000E-01 -0.53044200E+00
0.29761000E-01 0.13468000E-01
P 1 1.00
0.29761000E-01 1.0
D 8 1.00
0.72756200E+02 0.52000000E-04
0.10474200E+02 0.12626000E-01
0.62509000E+01 -0.63241000E-01
0.18018500E+01 0.23964700E+00
0.88845400E+00 0.38767200E+00
0.41566500E+00 0.35174400E+00
0.18308000E+00 0.20529000E+00
0.74233000E-01 0.54121000E-01
D 8 1.00
0.72756200E+02 -0.37000000E-04
0.10474200E+02 -0.15789000E-01
0.62509000E+01 0.78297000E-01
0.18018500E+01 -0.35829600E+00
0.88845400E+00 -0.47932500E+00
0.41566500E+00 0.18840700E+00
0.18308000E+00 0.57814500E+00
0.74233000E-01 0.29866000E+00
D 8 1.00
0.72756200E+02 -0.26000000E-04
0.10474200E+02 0.27189000E-01
0.62509000E+01 -0.13073800E+00
0.18018500E+01 0.83785700E+00
0.88845400E+00 0.73940000E-02
0.41566500E+00 -0.10612590E+01
0.18308000E+00 0.24900500E+00
0.74233000E-01 0.65356400E+00
D 1 1.00
0.74233000E-01 1.0
F 1 1.00
0.13040000E+01 1.0
F 1 1.00
0.43370000E+00 1.0
G 1 1.00
0.10772000E+01 1.0
```

Replace *ZZZ* with:

```
ECP60MDF 5 60
H-Komponente
1
2 1.000000 0.000000
S-H
2
2 14.604500 429.646087
2 7.218287 73.156884
P-H
4
2 11.577162 88.022917
2 10.883843 175.998196
2 6.424403 13.682274
2 5.224198 27.414651
D-H
4
2 7.699610 43.557852
2 7.550808 65.369108
2 3.961164 7.018596
2 3.872777 11.391733
F-H
2
2 3.379869 10.710220
2 3.326255 14.278125
G-H
2
2 5.452020 -11.651749
2 5.412585 -14.375525
```

Appendix B

NMR SPECTRA OF REPRESENTATIVE COMPOUNDS

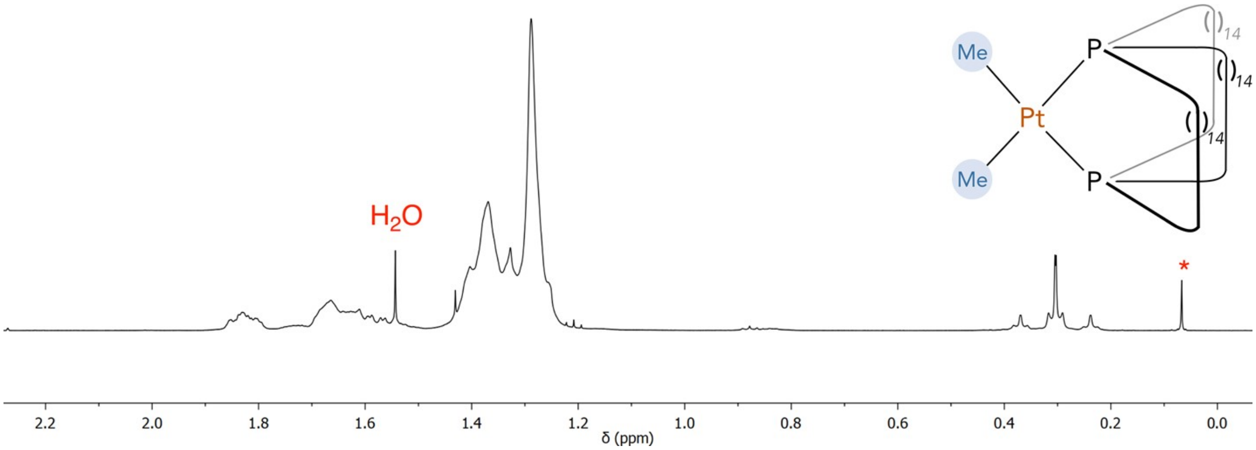

Figure s08. ^{1}H NMR spectrum of *cis*-**4c** (500 MHz, $CDCl_3$).

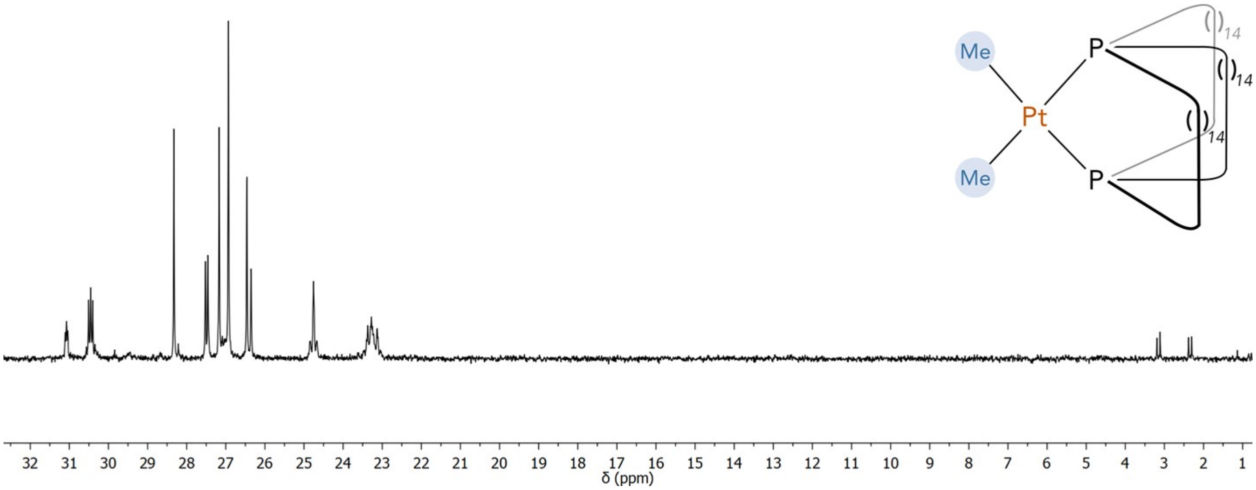

Figure s09. $^{13}C\{^{1}H\}$ NMR spectrum of *cis*-**4c** (500 MHz, $CDCl_3$).

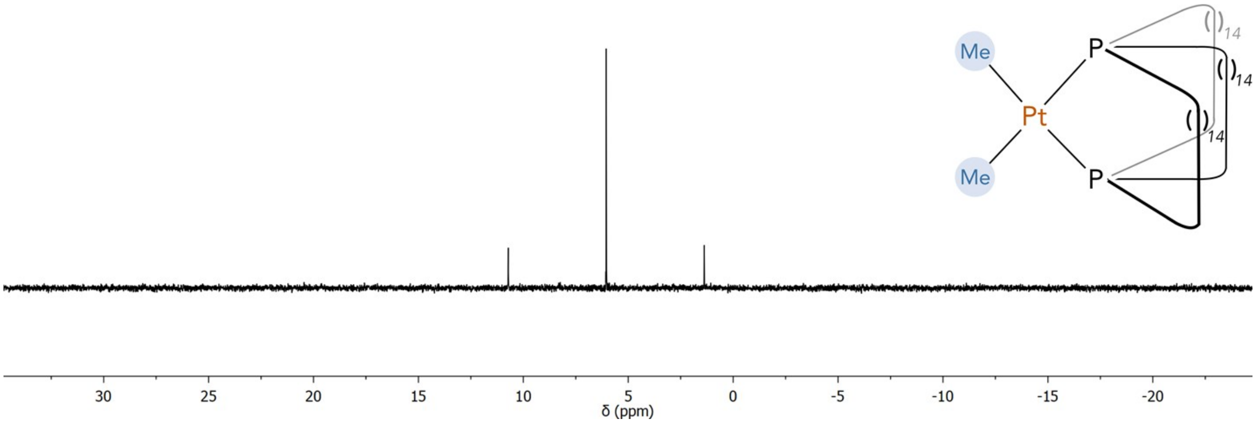

Figure s10. $^{31}P\{^{1}H\}$ NMR spectrum of *cis*-**4c** (500 MHz, $CDCl_3$).

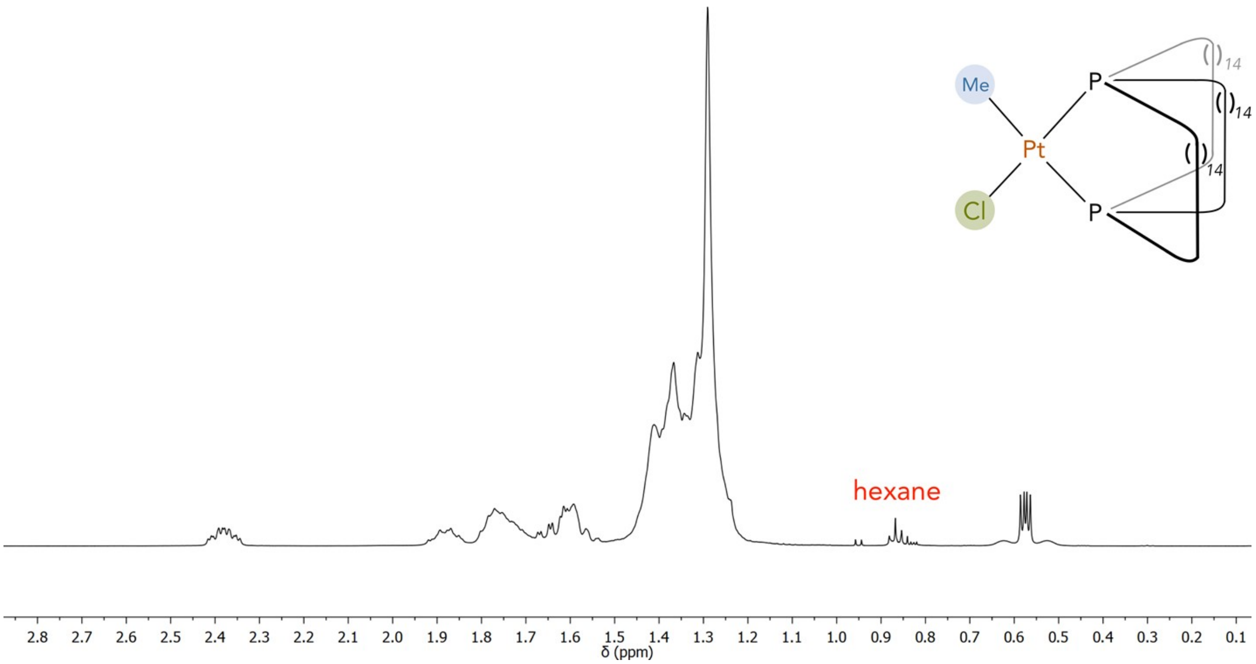

Figure s11. ^{1}H NMR spectrum of *cis*-**5c** (500 MHz, $CDCl_3$).

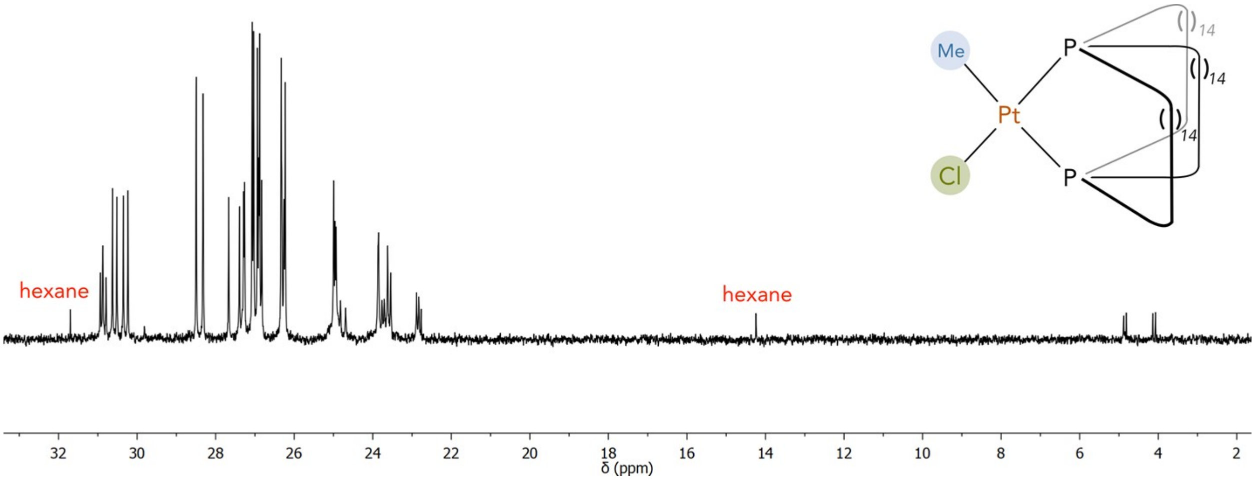

Figure s12. $^{13}C\{^1H\}$ NMR spectrum of *cis*-**5c** (500 MHz, $CDCl_3$).

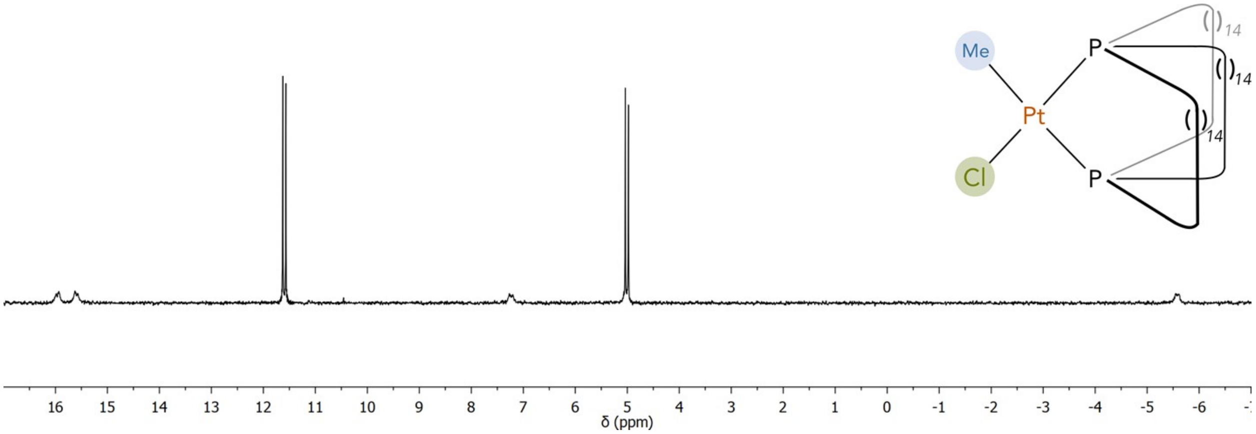

Figure s13. $^{31}P\{^1H\}$ NMR spectrum of *cis*-**4c** (500 MHz, $CDCl_3$).

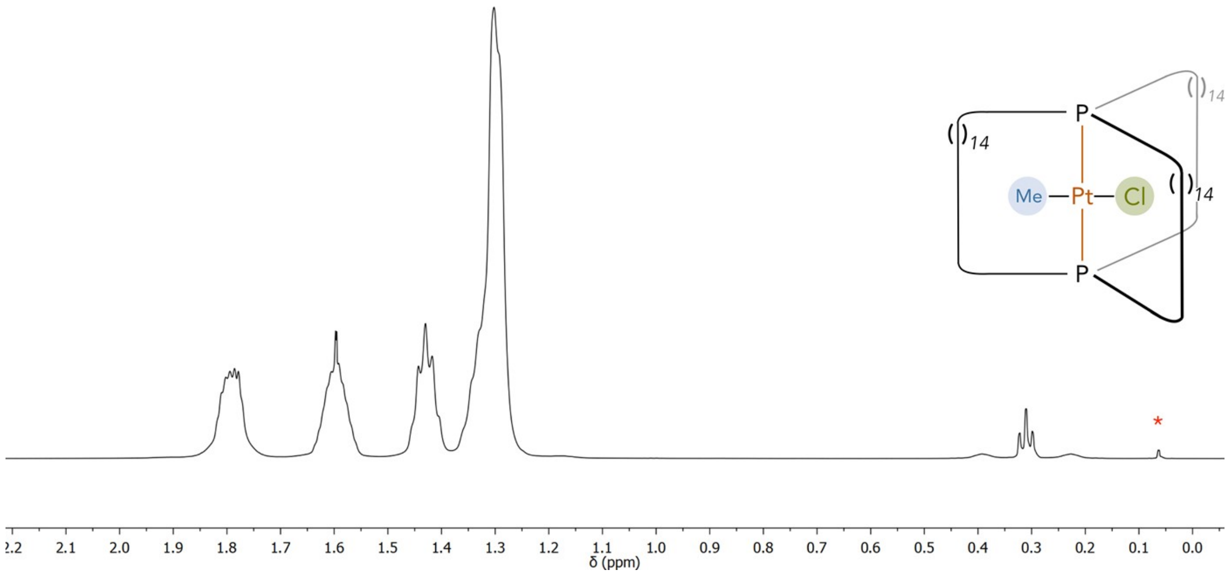

Figure s14. ^{1}H NMR spectrum of *trans*-**5c** (500 MHz, CDCl$_3$).

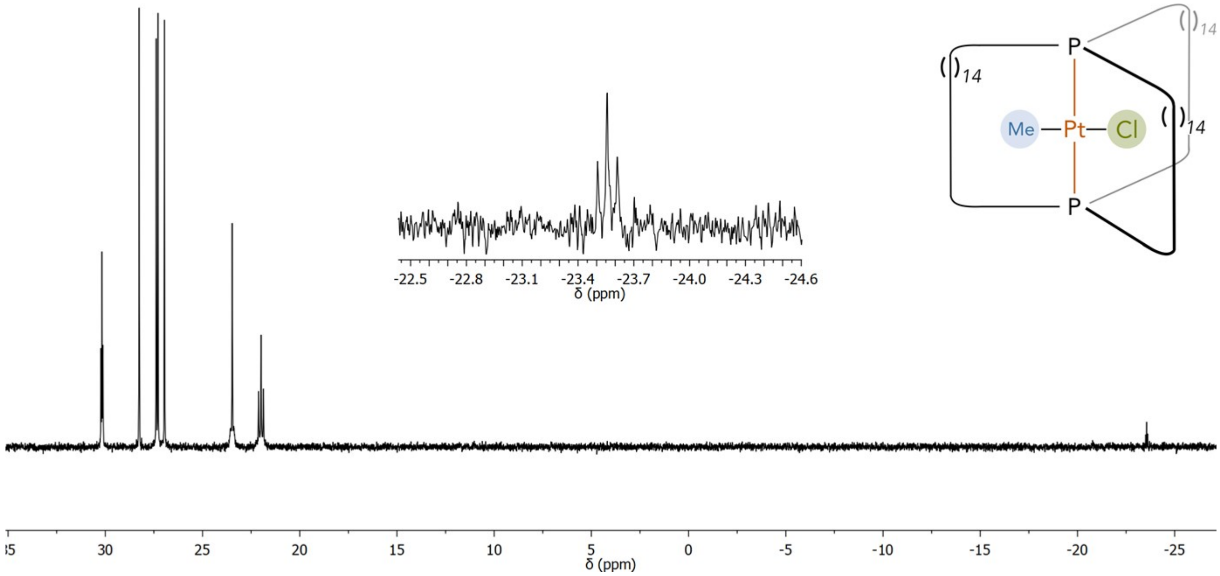

Figure s15. ^{13}C{^{1}H} NMR spectrum of *trans*-**5c** (500 MHz, CDCl$_3$).

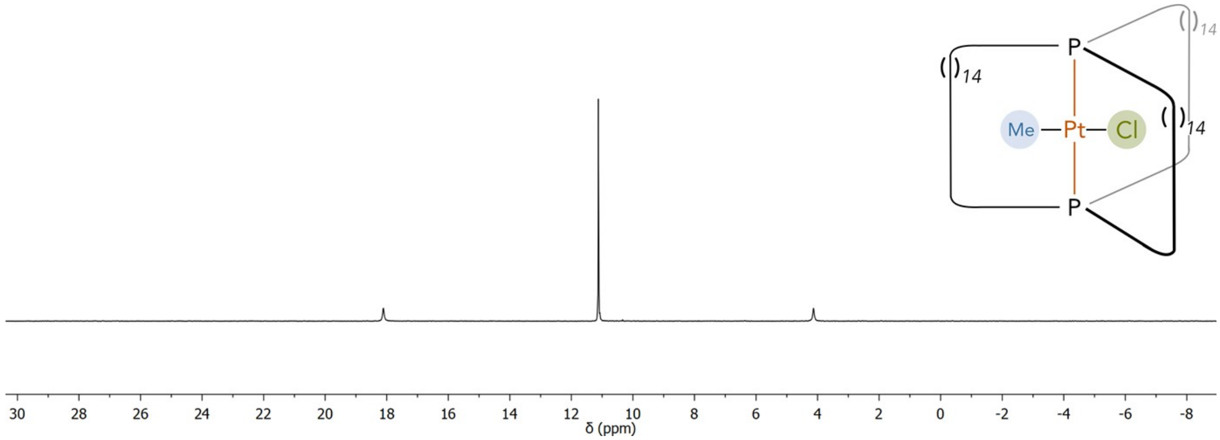

Figure s16. ^{31}P{^{1}H} NMR spectrum of *trans*-5**c** (500 MHz, CDCl$_3$).

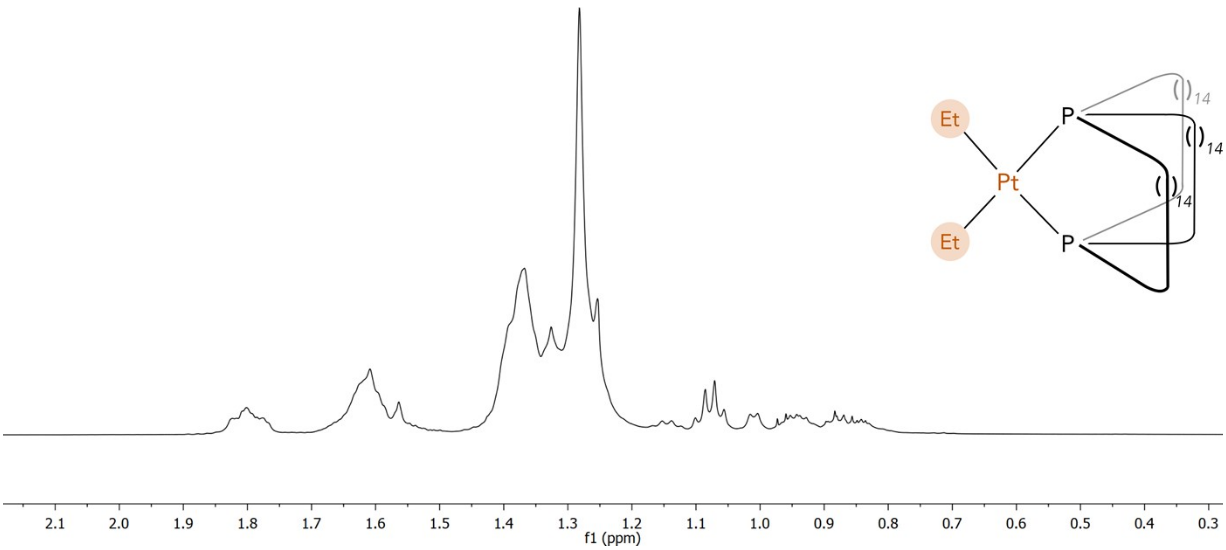

Figure s17. ^{1}H NMR spectrum of *cis*-**6c** (500 MHz, CDCl$_3$).

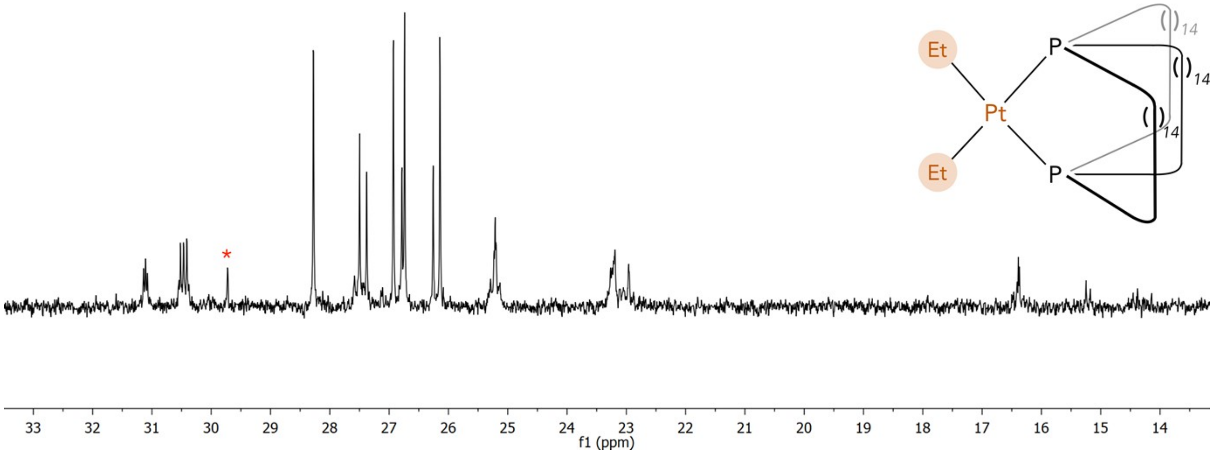

Figure s18. ^{13}C{^{1}H} NMR spectrum of *cis*-**6c** (500 MHz, CDCl$_3$).

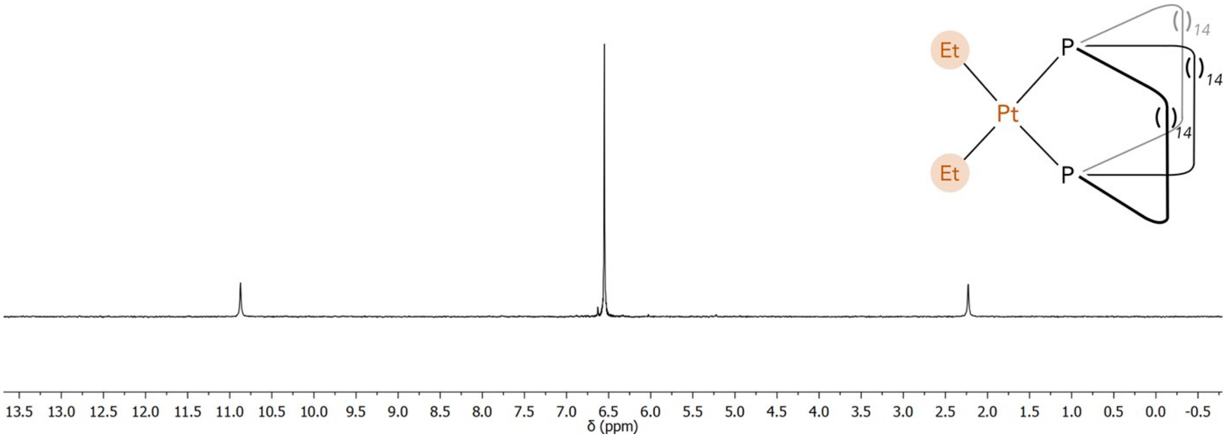

Figure s19. ^{31}P{^{1}H} NMR spectrum of *cis*-**6c** (500 MHz, CDCl$_3$).

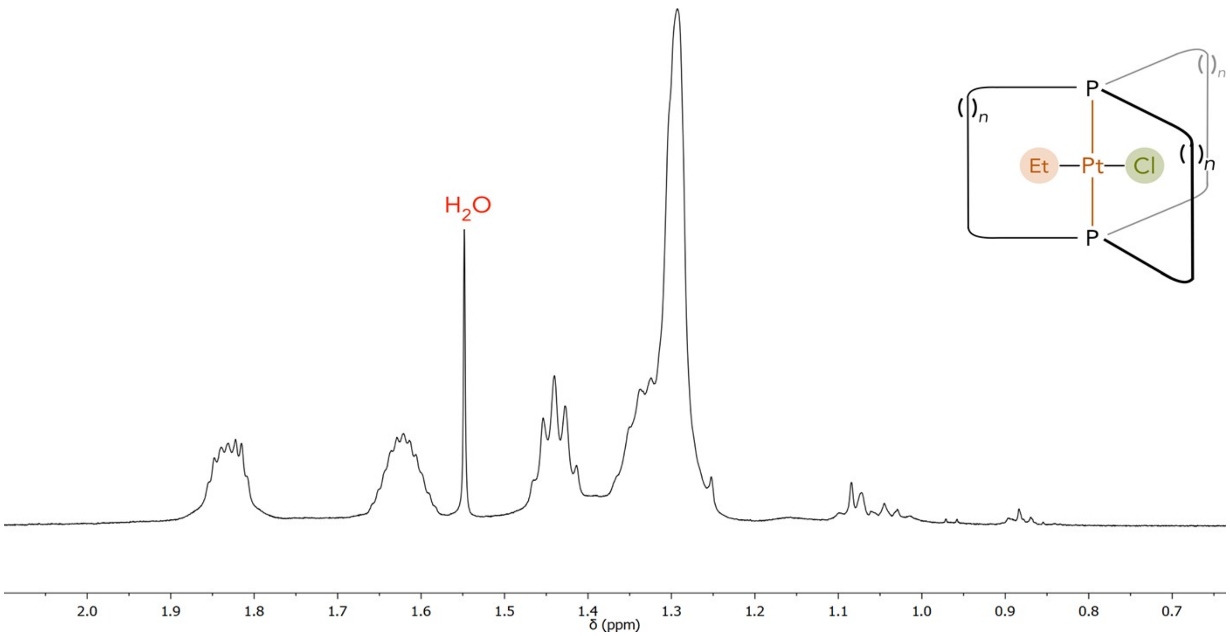

Figure s20. ^{1}H NMR spectrum of *trans*-**7c** (500 MHz, CDCl$_3$).

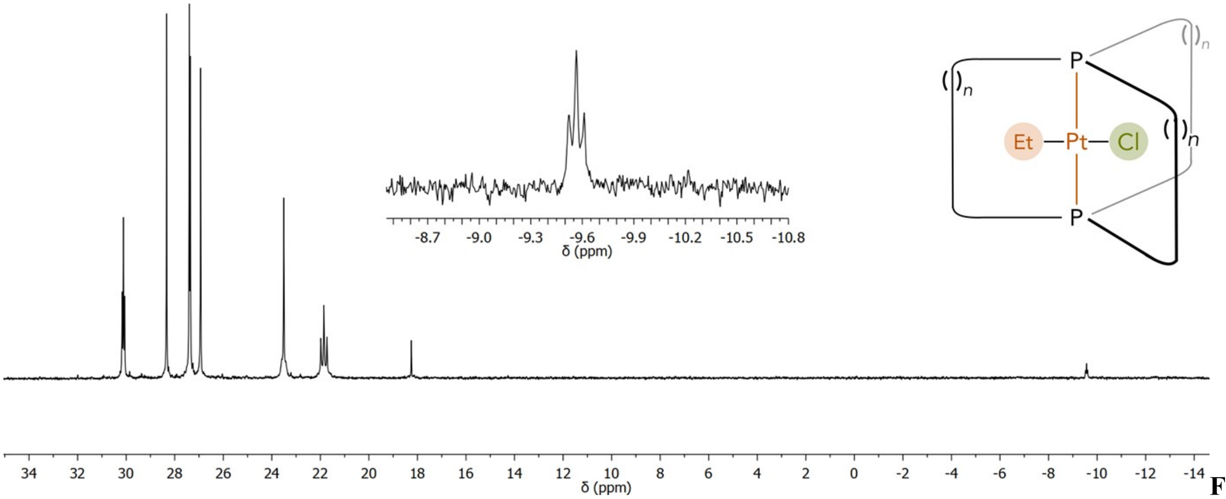

Figure s21. ^{13}C{^{1}H} NMR spectrum of *trans*-**7c** (500 MHz, CDCl$_3$).

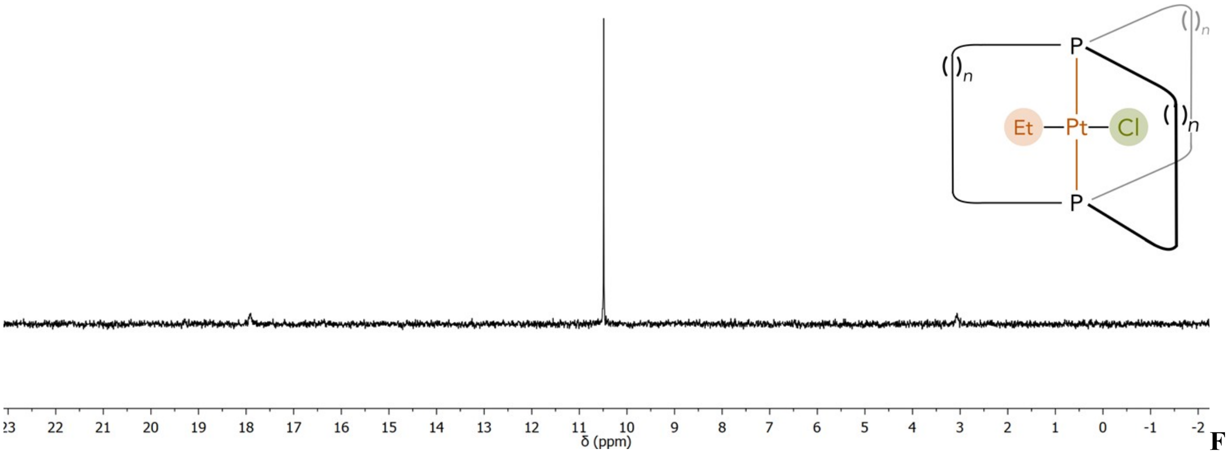

Fig

ure s22. ^{31}P{^{1}H} NMR spectrum of *trans*-**7c** (500 MHz, CDCl$_3$).

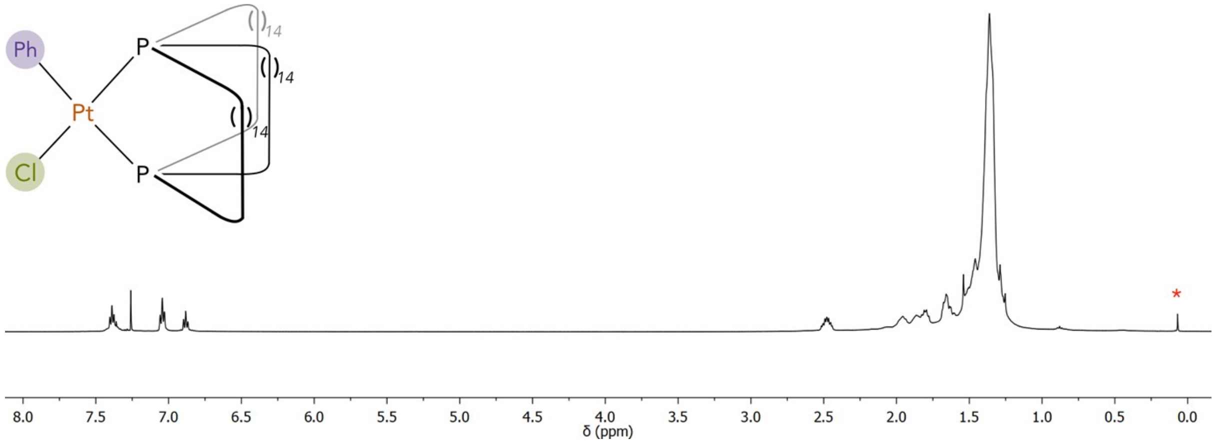

Figure s23. ^{1}H NMR spectrum of *cis*-**8c** (500 MHz, CDCl$_3$).

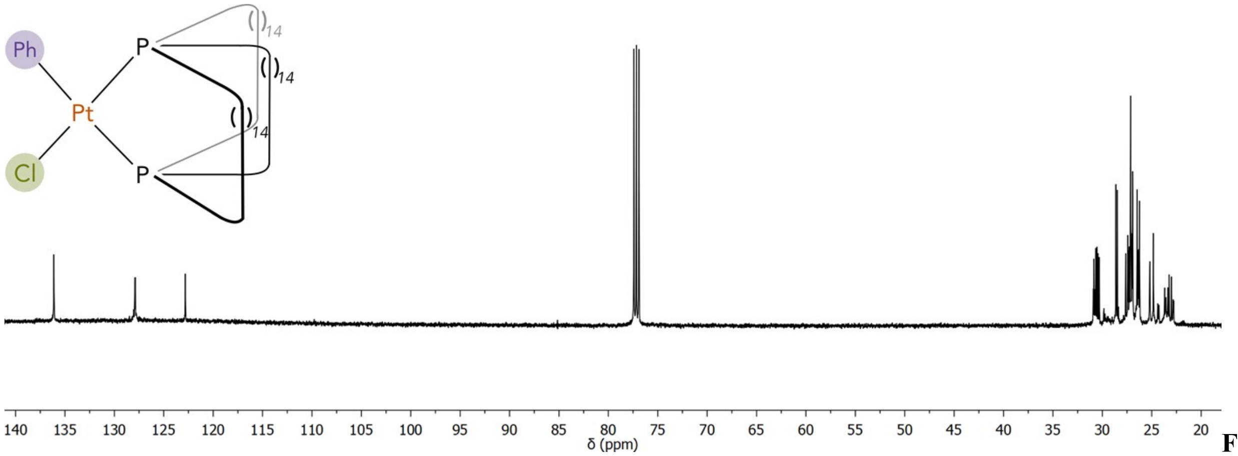

Figure s24. ^{13}C{^{1}H} NMR spectrum of *cis*-**8c** (500 MHz, CDCl$_3$).

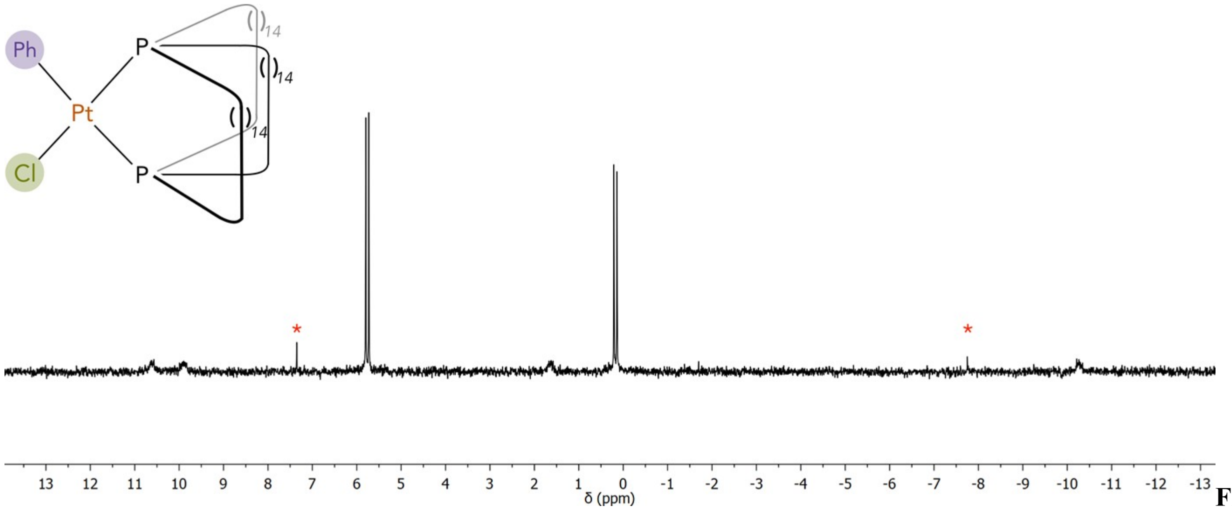

Figure s25. ^{31}P{^{1}H} NMR spectrum of *cis*-**8c** (500 MHz, CDCl$_3$).